

Differential Absorption Radar at 170 GHz for Atmospheric Boundary Layer Water Vapor Profiling

Richard J. Roy*, Ken B. Cooper, Matthew Lebsock, Luis Millán, Jose Siles, and Raquel Rodriguez Monje

Jet Propulsion Laboratory, California Institute of Technology, Pasadena, CA, USA

*richard.j.roy@jpl.nasa.gov

Abstract—We are developing a frequency-modulated continuous-wave (FMCW) radar between 167 and 174.8 GHz to measure differential absorption due to water vapor within the atmospheric boundary layer. In this work, we report on single-frequency measurements performed within this band in the presence of precipitating clouds. Despite the relatively low transmit power of 6-10 dBm, the high transmit/receive isolation and low noise figure of the system enables detection of radar echos from rain or clouds with high signal-to-noise ratio (SNR) out to about one kilometer. Near future upgrades to the system that will lengthen significantly the detectable range include a 15 to 20 dB increase in output power and 20 dB increase in antenna gain. This work builds on technology developed and measurements performed in our group in the 183.5 to 193 GHz band, which is subject to transmission restrictions due to passive remote sensing platforms that rely on those frequencies.

Keywords—Millimeter wave radar, Meteorological radar, Radar signal processing

I. INTRODUCTION

Passive satellite systems for measuring vertical water vapor profiles, including the Advanced Microwave Sounding Units (AMSUs) and the Atmospheric Infrared Sounder (AIRS), have limited ability to perform high-resolution observations in the presence of clouds, constituting an important gap in the global atmospheric remote sensing system [1], [2]. As a potential solution to this observational problem, we are developing a proof-of-concept, FMCW radar between 167 and 174.8 GHz to measure differential absorption due to the nearby 183 GHz water absorption line. By comparing the frequency dependence of the relative absorption between two given ranges with the known absorption line shape, we can retrieve absolute values of water vapor density as a function of radar range. From an airborne platform, this provides the opportunity to measure both in-cloud water vapor profiles *and* total column water vapor using the reflection from the Earth's surface.

Such a differential absorption radar (DAR) operating between 183.5 and 193 GHz was recently developed and successfully demonstrated in our group [3]. However, due to the abundance of passive remote sensors occupying this band, transmission is prohibited between 174.8 and 191.8 GHz [4]. Choosing the lower frequency band between 167 and 174.8 GHz is additionally attractive because of the ability to penetrate further into the atmosphere, making possible humidity measurements throughout the boundary layer. In fact, our modeling studies suggest that a DAR operating near 170 GHz can theoretically access the lower atmosphere even in the presence of strongly attenuating, warm rain [5].

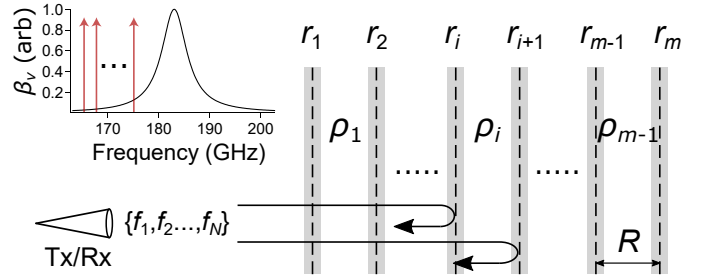


Fig. 1. Schematic of water vapor profile retrieval procedure. By comparing the frequency dependence between r_i and r_{i+1} of the specific attenuation $\beta_v \propto \rho$ with the absorption line shape (upper left), we can determine the mean water vapor density ρ_i .

II. DIFFERENTIAL MEASUREMENT BASIS

To understand the DAR measurement technique, we begin by writing the signal power received by the radar from range r at G-band frequency f as [3]

$$P_S(r, f) = G(f)Z(r)r^{-2}e^{-2\alpha(r, f)}, \quad (1)$$

where $G(f)$ represents the frequency-dependent gain of the system due to radar hardware, $Z(r)$ describes how the reflectivity varies with range,

$$\alpha(r, f) = \int_0^r (\sigma_v(r, f) + \sigma_{\text{part}}(r, f))dr \quad (2)$$

is the one-way attenuation of the radar beam [5], and we explicitly include the volumetric scattering r^{-2} dependence. Here σ_v and σ_{part} are the water vapor and particulate extinction coefficients, respectively, and we assume that the only relevant gaseous attenuation is that due to water vapor, as the atmospheric gaseous absorption in the band of interest is dominated by the water line at 183 GHz.

Then, taking the ratio of powers returned from two successive ranges r_1 and r_2 for the same frequency, and assuming that particulate extinction is independent of frequency over the relatively narrow band used, we have

$$\frac{P_S(r_2, f)}{P_S(r_1, f)} = \frac{Z(r_2)}{Z(r_1)} \left(\frac{r_1}{r_2}\right)^2 e^{-2\beta(r_1, r_2, f)R}. \quad (3)$$

In this equation $R = r_2 - r_1$ and we define β , the mean specific attenuation between points r_1 and r_2 with units of inverse distance. Note that because we assume σ_{part} is independent of frequency, its contribution to β is a

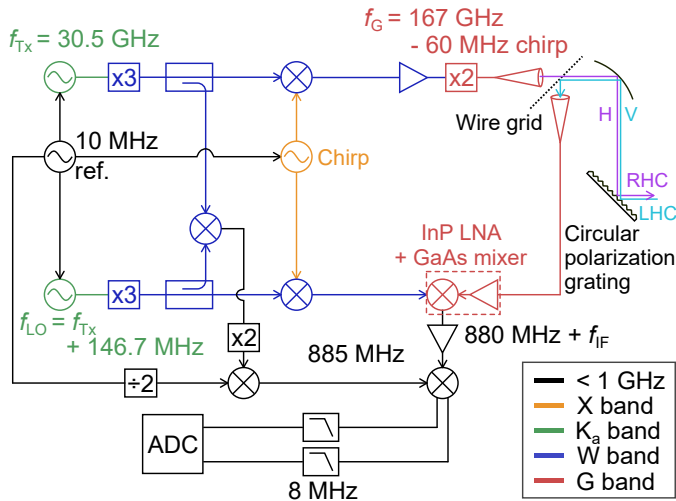


Fig. 2. High-level block diagram of the 170 GHz radar hardware. Different coaxial/waveguide sections are denoted by different colors (see legend).

frequency-independent offset. Thus, if we write $\beta(r_1, r_2, f) = \beta_v(r_1, r_2, f) + C(r_1, r_2)$, where the specific attenuation due to water vapor β_v is proportional to the water vapor density ρ , we can extract the mean water vapor density between r_1 and r_2 from the measured frequency dependence of the power ratio in (3). By following this protocol for a sequence of ranges $\{r_1, r_2, \dots, r_m\}$ given a set of transmit frequencies $\{f_1, f_2, \dots, f_N\}$, we retrieve the water vapor profile $\{\rho_1, \rho_2, \dots, \rho_{m-1}\}$ (see Fig. 1).

III. 167 - 174.8 GHz RADAR ARCHITECTURE

The block diagram of the 167-174.8 GHz radar hardware is shown in Fig. 2. Two phase-locked, K_a band synthesizer modules are frequency tripled and combined with an X band linear chirp waveform to drive the transmit and local oscillator (LO) chains of the radar front end. The resulting transmit and LO W band signals are frequency doubled in a GaAs frequency multiplier and subharmonic mixer, respectively, to generate the G band signals. By varying the transmit chain frequency f_{Tx} from 30.5 to 31.8 GHz, the resulting G band output frequency varies from 167 to 174.8 GHz and power from 6 to 10 dBm. The LO chain synthesizer frequency maintains a fixed offset from f_{Tx} of 146.7 MHz, resulting in a frequency offset at G band of 880 MHz. The linear chirp waveform is derived by up-converting a custom 1.00 to 1.03 GHz fast-sweeping synthesizer onto a phase-locked dielectric resonator oscillator (PLDRO) at 7 GHz. The final chirp bandwidth of $\Delta F_c = 60$ MHz and time of $\Delta t_c = 1$ ms result in a conversion from radar target range to intermediate frequency (IF) offset relative to the carrier (i.e. zero-range signal) of

$$f_{IF} = \frac{2r\Delta F_c}{c\Delta t_c} = r \times 0.4 \text{ kHz/m}. \quad (4)$$

The G-band portion of the receive chain features a custom InP low-noise amplifier (LNA) with $T_N = 500$ K and GaAs subharmonic mixer integrated into a single block.

To mitigate the effects of phase noise, we employ a high-isolation transmit/receive duplexing technique using a wire-grid polarizer (black dashed line in Fig. 2) and circular polarization grating [6], limiting the direct transmit leakage into the receive chain to -85 dB. Furthermore, after down-conversion of the FMCW signal to 880 MHz, the subsequent self-mixing in the I/Q demodulator with the reference signal ensures a high level of phase-noise cancellation, as detailed in [7].

This system maintains many aspects of the previous 183.5-193 GHz DAR system [3], with a notable exception being the offset of the zero-range FMCW radar echo from DC at baseband. As shown in Fig. 2, before down-converting the FMCW IF signal to baseband, the 10 MHz source is sent through a frequency divider and up-converted onto the 880 MHz phase-noise reference signal. Then, after I/Q demodulation, the zero-range radar signal appears at 5 MHz instead of DC. Without this baseband shift, the zero-range signal is corrupted by noise around DC, and is therefore filtered out and not used. With this setup, however, we can monitor the zero-range portion of the spectrum and potentially utilize it for calibration purposes.

IV. PRELIMINARY MEASUREMENTS OF PRECIPITATION

As a demonstration of the 170 GHz radar hardware described in Section III, we present measurements performed in the presence of rain and clouds on January 9, 2018 at the Jet Propulsion Laboratory (JPL). For these measurements, the radar was positioned inside a building and was pointing at an angle of 30 degrees relative to the ground into clouds/rain. Fig. 3 displays images of the rain and cloud conditions (a) and the radar front end platform (b). The measurement sequence involves setting the transmit synthesizer frequency to a desired value and performing 1000 consecutive, 1 ms long, 60 MHz chirps. At baseband, the in-phase (I) and quadrature (Q) signals are sampled at 26 MHz, resulting in 26000 points per chirp. The time-domain signal is then windowed with a Hanning window and zero-padded to 32768 points before performing the FFT to get the FMCW power spectra. We then average the 1000 individual measurements to obtain the final power spectrum.

A. FMCW Radar Spectra and Noise Floor Considerations

In order to obtain accurate water vapor density values using the method outlined in Section II, we must subtract off the contribution to the FMCW spectra from the noise floor. To see why this is, consider the detected power spectrum $P_D = P_S + P_N$, where P_S is the desired FMCW radar spectrum and P_N is a white noise spectrum. If we were to use the detected powers at two ranges in (3), we would find that the power ratio approaches unity for large range values where the SNR is small, implying that there is zero attenuation, and therefore, zero water vapor, between the two ranges. Moreover, because the variance of the white noise spectrum is small (see Fig. 4), the resulting incorrect estimate of zero humidity would have a small uncertainty.

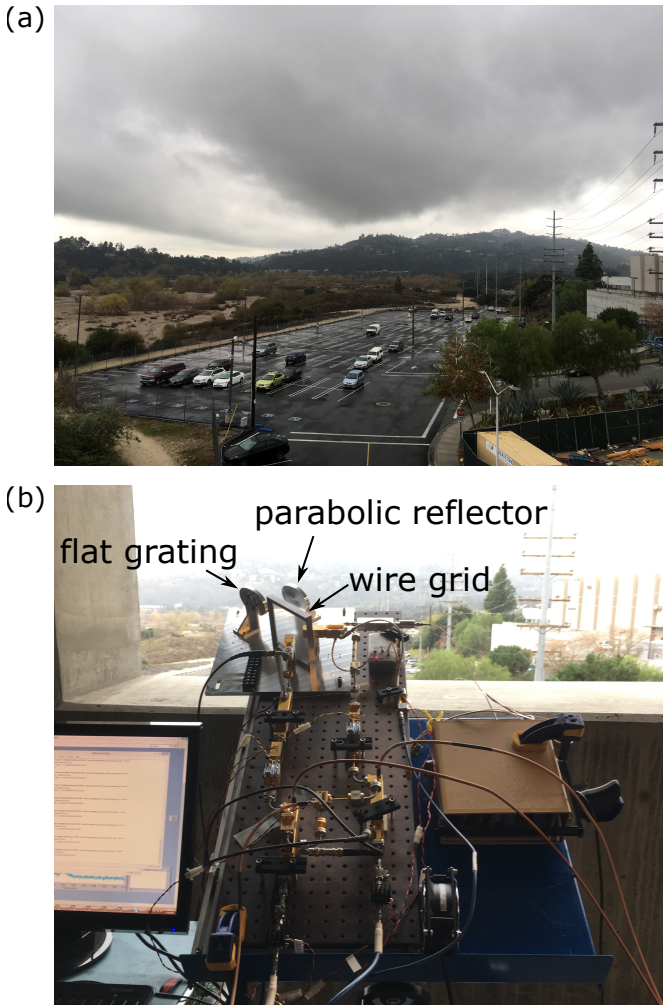


Fig. 3. (a) Cloud scene and (b) 170 GHz FMCW radar front end for measurements taken at JPL.

To account for this systematic underestimation of water vapor content, and to ensure that the variance of our signal power estimate becomes large in the low-SNR regime, we acquire identical measurements to those discussed above after all rain and clouds have cleared out, and subtract the resulting profiles $P_D - P_N$. In this case, P_N refers to all contributions to the detected power spectra that do not result from cloud or rain signals. Note that due to the slight frequency dependence of noise power spectrum, we cannot simply subtract a constant value for the noise spectral density from P_D in order to get P_S . This background noise floor subtraction is shown in Fig. 4a for a transmit frequency of 171.7 GHz, where we see that the variance in our estimate of P_S begins steadily increasing after the signal power crosses the noise floor.

The resulting power spectra power spectrum at 171.7 GHz scaled by the square of the range and normalized to its value at 50 meters is shown in Fig. 4b. The r^2 scaling eliminates the power decay due to volumetric scattering range dependence, and elucidates the structure of the quantity $Z(r) \exp(-2\alpha(r, f))$ (see (1)). Thus, the observed decay

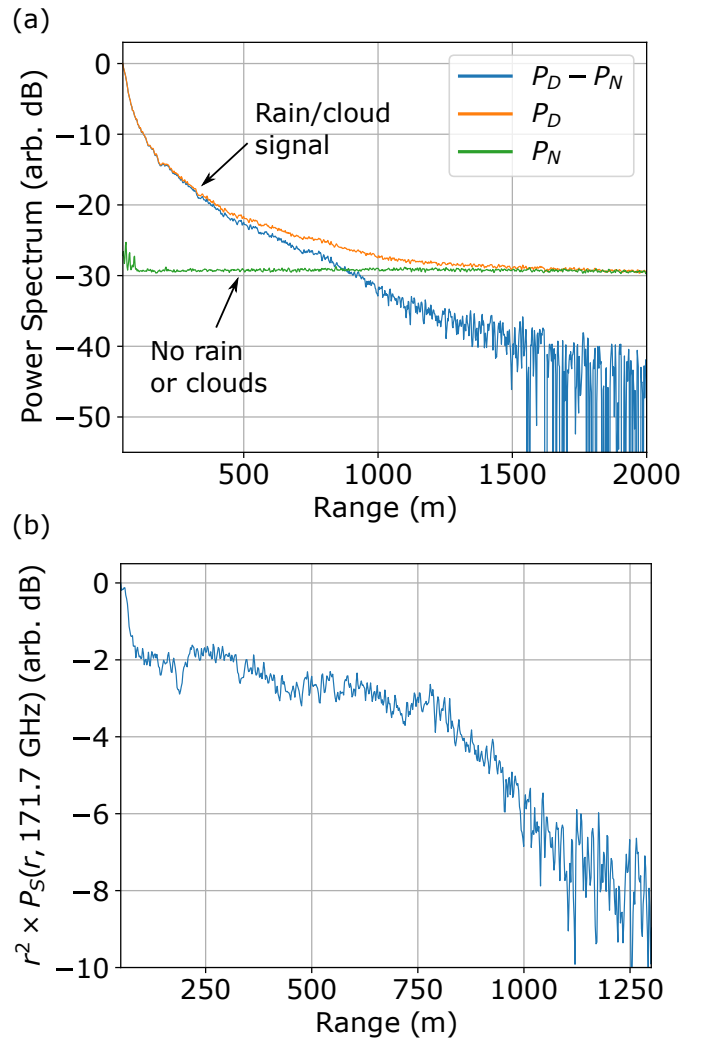


Fig. 4. (a) Noise floor subtraction at $f = 171.7$ GHz. The noise floor power spectrum (green trace) is acquired after the rain and clouds clear out, with the transmitter on. The received power spectrum frequency axis is converted to range using (4). (b) Signal power spectrum from (a) scaled by r^2 .

versus range in this plot stems from either particulate extinction or absorption due to water vapor. Compared to the roughly 300 meter range with $\text{SNR} > 1$ observed in the 183.5-193 GHz DAR system [3], the results in Fig. 4 are quite promising for future airborne measurements probing the lower atmosphere, which will feature higher transmit power and antenna gain.

V. CONCLUSION

The FMCW radar architecture and measurements reported here form an important starting point for future airborne measurements of water vapor profiles within the planetary boundary layer. The roughly 1 km range exhibiting a high SNR will increase significantly with a 15-20 dB increase in output power and 20 dB increase in antenna gain. Future measurements to be presented will include fast switching of the transmit frequency over the 167 to 174.8 GHz band in order to measure the differential absorption and extract humidity.

Further future potential improvements to the measurement system include a study to optimize the choice of transmit frequencies, and including coincident passive measurements of brightness temperatures near the 183 GHz water line to further constrain the humidity profile retrieval and to provide continuous humidity measurements in the aircraft when passing from cloudy to clear-sky regions, where the only radar signal comes from the Earth's surface.

ACKNOWLEDGMENT

The research was carried out at the Jet Propulsion Laboratory, California Institute of Technology, under a contract with the National Aeronautics and Space Administration. Copyright 2018 California Institute of Technology. U.S. Government sponsorship acknowledged.

REFERENCES

- [1] T. J. Greenwald and S. A. Christopher, "Effect of cold clouds on satellite measurements near 183 ghz," *Journal of Geophysical Research: Atmospheres*, vol. 107, no. D13, pp. AAC 3-1-AAC 3-8, 2002.
- [2] E. J. Fetzer, B. H. Lambriksen, A. Eldering, H. H. Aumann, and M. T. Chahine, "Biases in total precipitable water vapor climatologies from atmospheric infrared sounder and advanced microwave scanning radiometer," *Journal of Geophysical Research: Atmospheres*, vol. 111, no. D9, 2006.
- [3] K. B. Cooper, R. R. Monje, L. Millán, M. Lebsock, S. Tanelli, J. V. Siles, C. Lee, and A. Brown, "Atmospheric humidity sounding using differential absorption radar near 183 ghz," *IEEE Geoscience and Remote Sensing Letters*, vol. 15, no. 2, pp. 163-167, Feb 2018.
- [4] *Manual of Regulations and Procedures for Federal Radio Frequency Management*, from the National Telecommunications & Information Administration, 2015 Revision of the May 2013 Edition.
- [5] M. D. Lebsock, K. Suzuki, L. F. Millán, and P. M. Kalmus, "The feasibility of water vapor sounding of the cloudy boundary layer using a differential absorption radar technique," *Atmospheric Measurement Techniques*, vol. 8, no. 9, pp. 3631-3645, 2015.
- [6] K. B. Cooper, N. Llombart, G. Chattopadhyay, B. Dengler, R. E. Cofield, C. Lee, S. Filchenkov, and E. Kuposova, "A grating-based circular polarization duplexer for submillimeter-wave transceivers," *IEEE Microwave and Wireless Components Letters*, vol. 22, no. 3, pp. 108-110, March 2012.
- [7] K. B. Cooper, R. J. Dengler, N. Llombart, B. Thomas, G. Chattopadhyay, and P. H. Siegel, "Thz imaging radar for standoff personnel screening," *IEEE Transactions on Terahertz Science and Technology*, vol. 1, no. 1, pp. 169-182, Sept 2011.